Proximity Nuclear Decay

Alan McIntosh

Research Advisor: Romualdo de Souza

Nuclear Chemistry
Indiana University Dept. of Chemistry and
Indiana University Cyclotron Facility
Bloomington IN USA

22 April 2005

INTRODUCTION

This report consists of two parts. In the first section, I describe a simulation to explain a recently observed trend in the average transverse energy of isotopically resolved fragments emitted in a nuclear reaction. Following a description of the experimental observations, a model is described that relates the observations to proximity decay. Developing, debugging, and using a simulation based on this physical scenario constituted of a major portion of my C500 project. In the second section of this report, the testing of detectors for an upcoming experiment is described.

SECTION I: PROXIMITY DECAY SIMULATIONS

Experimental Observations and Hypotheses

In a recent paper [1], an enhancement of the average transverse energy, $\langle E_T \rangle$ for neutron deficient isotopes of odd-Z elements as compared to other isotopes of the same element was observed (Figure 1). The cause of this enhancement has sparked much debate. A physical picture of proximity decay consistent with the available data has been proposed [1], stimulating the investigation of this physical picture with a simulation.

Figure 1 shows the average transverse energy, $\langle E_T \rangle$, as a function of mass number (A) for isotopically resolved light-fragments observed in a reaction of ^{114}Cd + ^{92}Mo at E/A = 50 MeV. The three panels show the $\langle E_T \rangle$ vs. A for particles emitted from the mid-velocity region in both central and mid-peripheral (MP) collisions and particles emitted from the excited projectile-like fragment (PLF*) in a MP collision. Mid-velocity fragments are those with velocities intermediate projectile-like and target-like (TLF*) nuclei that result from the collision. In all cases, as the atomic number Z increases, $\langle E_T \rangle$ increases. This trend, evident in Figure 1, may be understood as increased coulomb repulsion between the emitted particle and a decay residue with increasing atomic number of the emitted particle. Moreover, the trend in mass number A as well as Z may be understood more generally as the interplay of coulomb repulsion, thermal motion, and possibly collective expansion. Since the thermal component is mass independent and the coulomb component is dependent only on charge, it is possible to disentangle these effects by examining $\langle E_T \rangle$ for different isotopes of an element. As the mass increases for a given element, $\langle E_T \rangle$ tends to stay about the same or decrease slightly. As mass-

dependent collective flow would predict an increase in $\langle E_T \rangle$ with increasing mass, the results indicate that effects of collective flow are negligible. For the lightest isotopes of even-Z elements however, there is a significant enhancement in $\langle E_T \rangle$, suggesting that there is another factor at work.

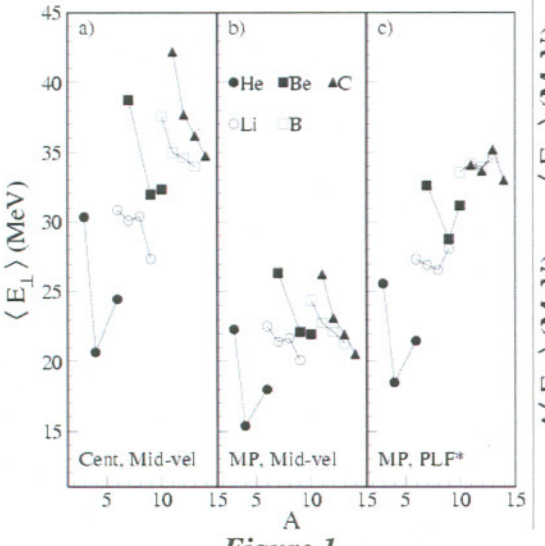

Figure 1

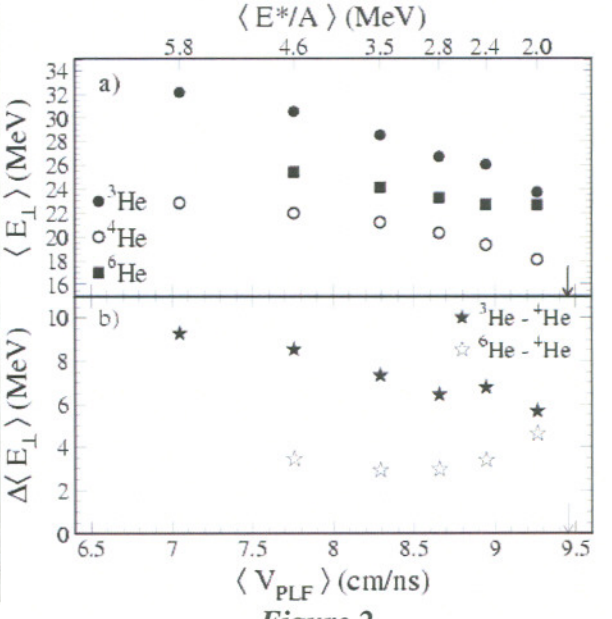

Figure 2

*Figure 1 shows an enhancement in the average transverse energy for the neutron deficient isotopes of even-Z elements. Figure 2 shows that this enhancement increases with increasing excitation energy of the PLF**

It has been hypothesized that the enhancement in $\langle E_T \rangle$ for neutron-deficient isotopes is related to the average emission times. If a particle is emitted early while the PLF* is still very hot, the emitted particle will have a high initial velocity due to the great amount of thermal motion; conversely, a late emission (from a cooler PLF*) will result in the emitted particle having a lower kinetic energy. Since the neutron-deficient isotopes are more tightly bound, they are more likely to be emitted early while the PLF* is still hot, and thus on average will have a higher kinetic energy. This physical scenario, however, would predict that as the excitation energy is increased, the emission rate of all

species increases making the emission time distributions narrower and comparable for all isotopes. Hence, any difference in $\langle E_T \rangle$ between the isotopes due to differences in emission times should decrease as excitation of the PLF* increases. Figure 2 shows the opposite trend. By using calorimetry, the velocity damping of the PLF* is related to its excitation energy [2]. In the upper panel of Figure 2, $\langle E_T \rangle$ for isotopes of helium are plotted as a function of PLF velocity. The deduced excitation energy is shown at the top of the figure. To illustrate the $\langle E_T \rangle$ enhancement clearly, the difference in $\langle E_T \rangle$ for different helium isotopes is shown in the lower panel. As the excitation of the PLF* increases, the difference between the $\langle E_T \rangle$ of ^{3}He and the $\langle E_T \rangle$ of ^{4}He increases (closed stars) while the difference for ^{6}He and ^{4}He remains constant after a small initial decrease (open stars). This evidence suggests that the displacement of the emission time can not be the origin of the enhancement in $\langle E_T \rangle$ in neutron-deficient isotopes.

It has recently been proposed [1] that the enhancement of $\langle E_T \rangle$ for fragments with N<Z is due to the proximity decay of emitted particles. A particle emitted from the PLF* is not necessarily in the ground state, and, if excited, can decay by particle emission before being detected. If the emitted particle is β-stable or neutron-rich, the most likely decay channel is neutron emission, as a neutron has no coulomb barrier toward emission. For neutron-deficient isotopes however, charged particle decay is favored over neutron emission since emission of a neutron by a neutron-deficient fragment would result in the creation of a less stable species at a high energy cost, making this type of decay unfavorable at high energy and impossible at low energy. The kinetic energy of a fragment produced via charged particle decay reflects the energy gained by its more highly charged parent in the field of the PLF*. Thus, a particle can be expected to have a

larger kinetic energy if produced through charged particle decay than if directly emitted from the PLF*. Naturally, the parent fragment must have a lifetime sufficiently long to acquire a significant amount of kinetic energy before decaying. The impact of charged particle decay on the kinetic energy of the observed particles can understood by considering two systems: (1) in which ^{7}Be is emitted from the PLF*, and (2) in which the PLF* emits ^{11}C which subsequently decays into an alpha particle and a ^{7}Be. Assume, for simplicity, that the emitted particles have no initial velocity. Figure 3 shows the 1/r potential felt by ^{11}C and by ^{7}Be as a function of position. The ^{7}Be in case 2 feels, at the instant of its emission, a certain potential. As the two body system evolves in time, the ^{7}Be can be seen to "roll down" the curve (i.e. it is repelled from the PLF*), its potential energy being converted to kinetic. After a sufficient amount of time, all of the potential energy has been converted to kinetic. In case 1, the ^{11}C feels a higher initial potential. The ^{11}C is repelled from the PLF*, following the upper potential curve, until it decays. After decay, we follow the newly created ^{7}Be as it "rolls down" the lower potential curve. Neglecting the recoil from the alpha particle, the final kinetic energy of the ^{7}Be in case 2 will be the sum of the energy it acquired before decay ($V_{\text{before decay}}$ in Figure 3) and the energy it acquired after decay ($V_{\text{after decay}}$). It is clear that the kinetic energy of the ^{7}Be produced through via secondary charged particle decay is greater than the kinetic energy of the ^{7}Be produced by direct emission from the PLF*. Since the charged particle decay channel should only be a factor for neutron-deficient isotopes, and since the probability of production of excited particles from the PLF* increases with increasing excitation energy, this physical scenario is consistent with the trend shown in Figure 2.

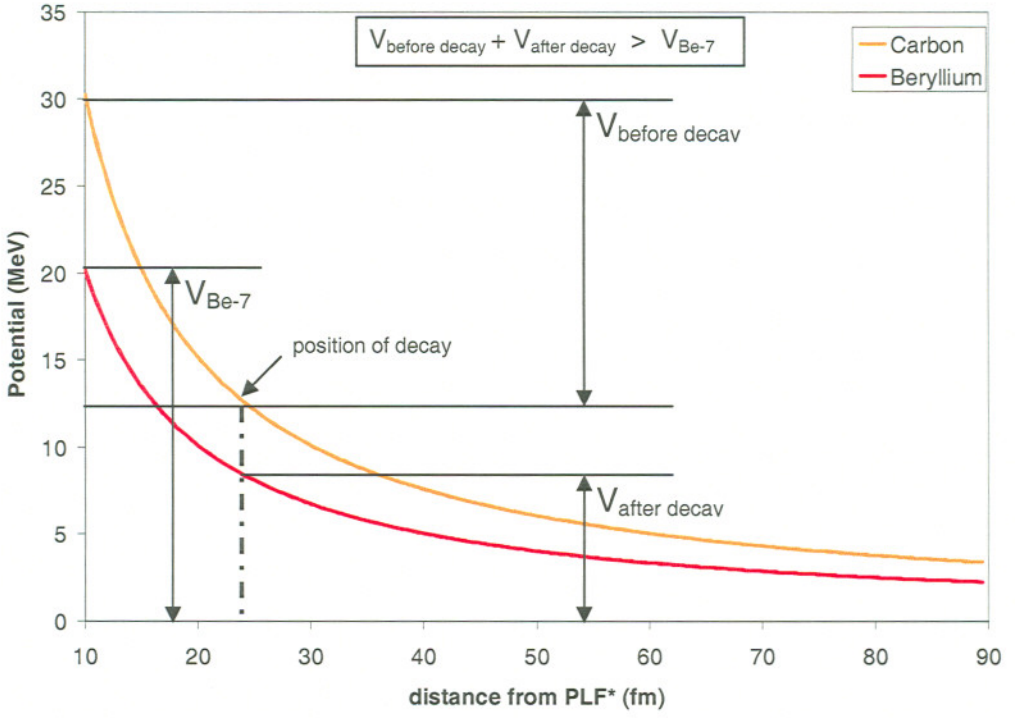

Figure 3

Fragments produced through secondary charged particle decay in the proximity of the emitting nucleus reflect the coulomb repulsion of the primary fragment and hence have higher kinetic energy than fragments of the same charge not produced through charged particle decay.

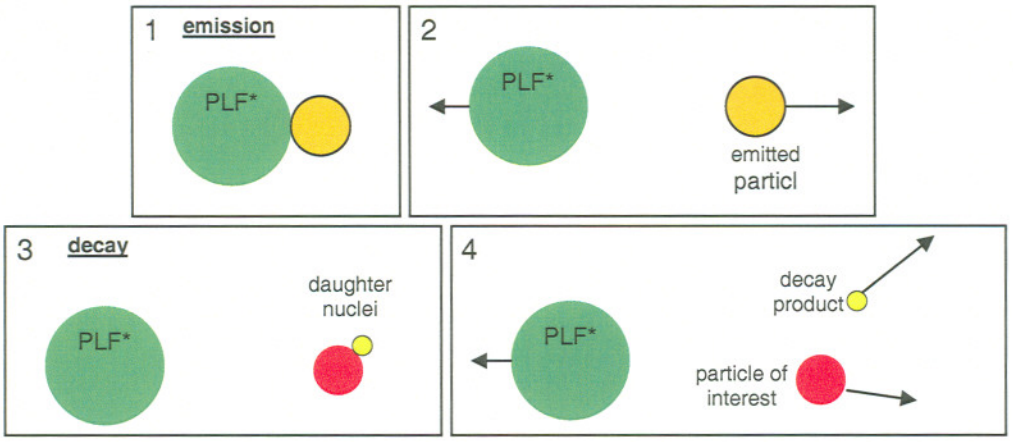

Figure 4

A cartoon of the charged particle decay explains the nomenclature subsequently used in discussion. In emission, *the PLF* ejects the* emitted particle. *After some time,* decay *occurs, in which the emitted particle becomes the two* daughter nuclei *designated the* decay product *and the* particle of interest.

Effect of Decay Direction and Lifetime on Kinetic Energy

This simple model is complicated by the recoil of the particle of interest from the decay product. The direction of decay has a strong impact on the kinetic energy of the particle of interest. Moreover, the decay can not always be considered isotropic due to tidal effects. Figure 4 illustrates the physical scenario previously described and clarifies the nomenclature used in the remainder of this report.

Since the longer the emitted particle exists in the field of the PLF* the more energy it will acquire (up to its asymptotic value), the transverse energy of the particle of interest should increase and approach a constant as a function of the lifetime of the emitted particle. Plots of transverse energy vs. lifetime for various cases of emission and decay angles are shown in Figure 5. The transverse energy is arbitrarily chosen to be the energy due to velocity in the x-y plane. These were produced using the simulation described in this paper. While two of the cases shown here produce the expected result, one clearly does not.

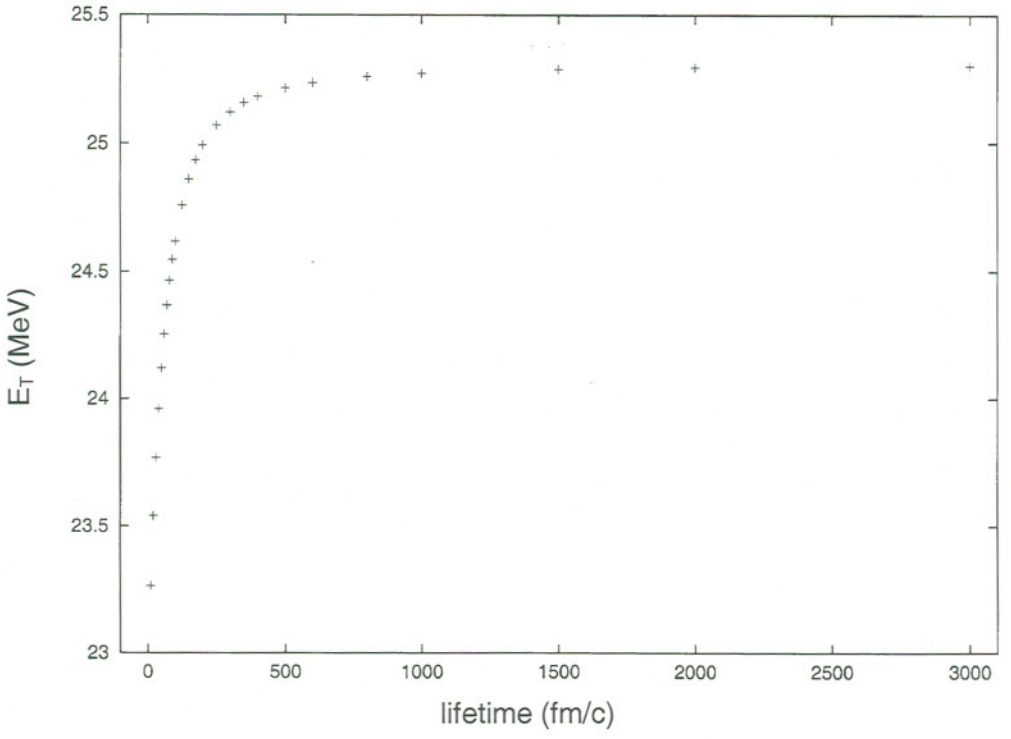

Figure 5a

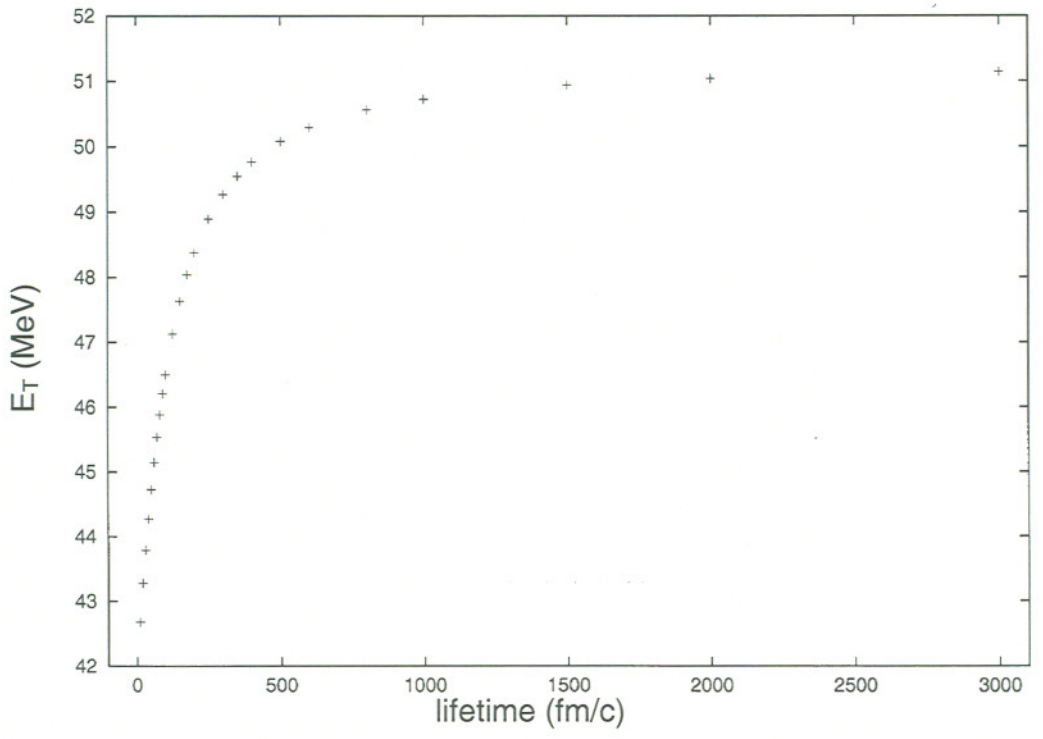

Figure 5b

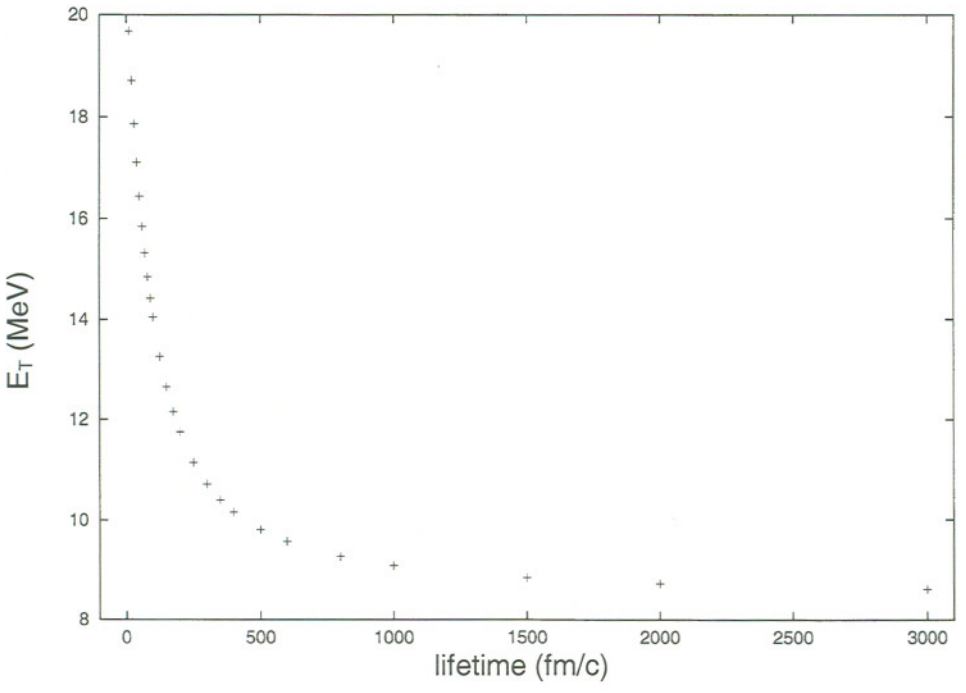

Figure 5c

The transverse energy (MeV) of the particle of interest is plotted as a function of its lifetime (fm/c) for various angles of emission and decay. In all three panels, emission occurs perpendicularly to the beam direction. In Figure 5a, decay occurs perpendicularly to emission (in the beam direction). In Figure 5b decay occurs in the same direction as emission, with the particle of interest furthest from the PLF. In Figure 5c, the decay occurs in the same direction as the emission, with the particle of interest closest to the PLF*.*

Moreover, the magnitude of the effect in the longitudinal decay cases (15MeV, Figures 5b & 5c) is cause for concern, since the potential energy of the two daughters at the instant of decay is on the order of 2 MeV. However, the large difference in energy does in fact have a physical origin. Since these particles are moving relative to the center of mass frame of the system, they have some transverse velocity, the square of which is proportional to their transverse energy. If the velocities are large, a minor change in their velocities will produce a large change in their energy. If instead we look in the center of

mass of the two daughters, the same small change in their velocities will not produce as great a change in their kinetic energies.

The decrease in E_T as a function of lifetime shown in Figure 5c makes physical sense as well: the energy of the particle of interest is being decreased by the decay product exerting a force in the direction opposite to its velocity. If the decay occurs far from the PLF* where the field is negligible, the particle of interest recoils from the decay product and loses some of its kinetic energy. If the decay occurs in the field of the PLF*, the PLF* pushes the decay product away from the particle of interest, thus preventing the decay product from having as much influence on the particle of interest. The transverse decay case (Figure 5a) shows that when the recoil of the ^{7}Be is perpendicular (i.e. does not effect) the transverse velocity, an average enhancement in E_T is observed which is dependent on the lifetime of the emitted particle in the field. Moreover, it is clear from these figures that the angle of decay has a large effect on the average transverse energy.

The Tidal Effect: A Simple Model

To understand the behavior of a charge distribution in a non-uniform external field, tidal effects must be considered. Tidal effects were first involved in understanding the dependence of the energetics of gravitational systems with respect to different orientations of a mass distribution in an external gravitational field. Tidal effects may be applied analogously to charge distributions in an electric field.

Consider the PLF* and the emitted particle at some separation distance. The decay of the emitted particle into two daughter nuclei can be described as the formation of a dipole. This dipole will clearly have preferred orientations in the field of the PLF*.

Calculating the sum of the potential between the PLF* and each of the two daughter particles, we find that it differs from the potential between the PLF* and the emitted particle, even though the center-of-charge has been preserved. Specifically, we find that the change in the potential varies with the angle between the emission direction and the decay direction. Figure 6 illustrates schematically how the potential of the system can change due to dipole orientation despite the center-of-charge remaining fixed. It is crucial that the center-of-charge remain fixed, as the center-of-charge is propagating in the coulomb field of the PLF* and a sudden change in the position of the center-of-charge would alter the total energy of the system in a physically unrealistic way. Figure 7 shows the difference in potential for the PLF*/ emitted particle system and the PLF*/ two daughters system as a function of angle (φ) for different distances between the PLF* and the emitted particle (r):

$$V(\phi,r)=V_{^{7}Be}^{PLF^*}(\phi,r)+V_{^{4}He}^{PLF^*}(\phi,r)-V_{^{11}C}^{PLF^*}(r)$$

The PLF* is taken to be ^{86}Br, the emitted particle ^{11}C, the particle of interest ^{7}Be, and the decay product ^{4}He.

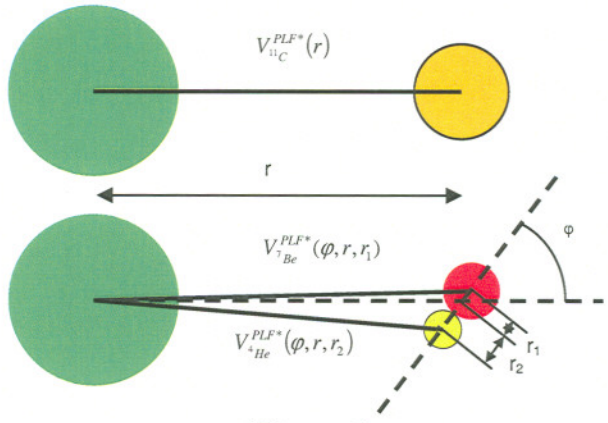

Figure 6

Cartoon illustrating the effect of the angle of decay on the potential between each of the daughters and the PLF. Here, r refers to the distance from the center of the source nucleus to the center-of-charge of the two daughters. The distance between the two daughters is held constant.*

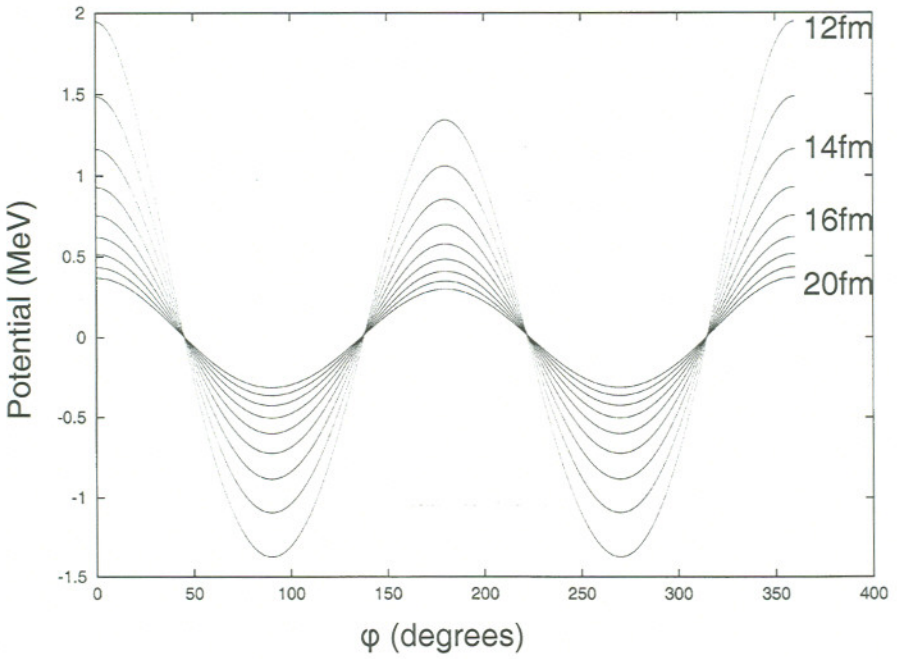

Figure 7
Potential (MeV) as a function of orientation of the dipole (degrees). Transverse decay orientations are energetically favorable as compared to longitudinal. φ (degrees) is the angle between the emission direction and the decay direction. The plot shows this function for different distances (r in Figure 6) from 12 to 20 fm.

Longitudinal decays (0° and 180°) are the most energetically unfavorable while transverse decays (90° and 270°) are the most favorable. Predictably, the difference in configurational potential for transverse and longitudinal decay decreases with increasing distance from the PLF*. It is interesting to note that 180° decay (designated "near" decay, since the particle of interest is nearer to the PLF* than the decay product) is slightly more favorable than 0° decay (designated "far" decay). This difference appears to be due to two opposing effects, which are explored in Figure 8.

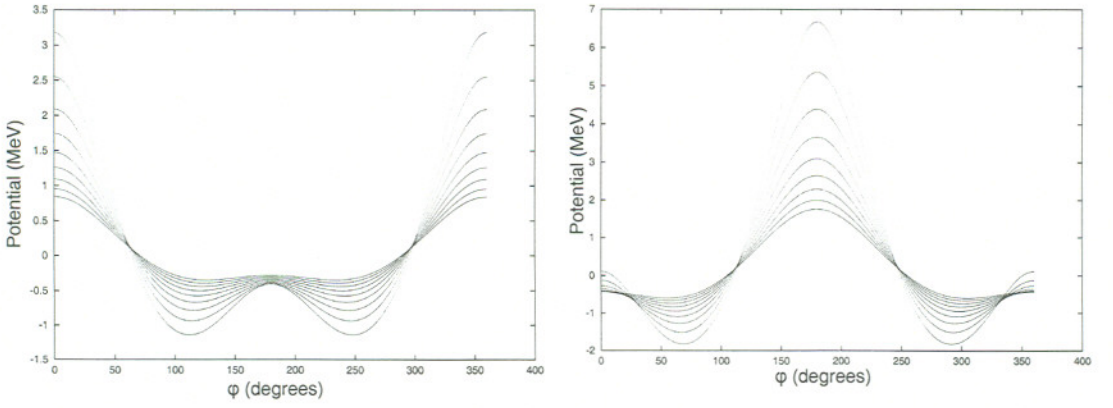

Figure 8
The left pane is for a dipole of two equal charges rotated asymmetrically. The right pane shows an unequal dipole rotated symmetrically. The true physical picture is a composite of these effects.

As previously stated, it is essential to preserve the center-of-charge distance in the external field. Varying the center-of charge distance changes the monopole term of the interaction with the field. To consider the orientation of the dipole, it is necessary to fix the monopole term. In Figure 8, we seek to disentangle the effect of asymmetrically rotating the dipole (rotating the dipole about its center-of-charge rather than about the midpoint) from the effect of the asymmetry of the dipole (the two charges are not equal). The preference of decay at certain angles shown in Figure 7 can be understood by examining these two underlying effects, though it should be noted that by forcing a symmetric dipole to rotate asymmetrically, or forcing an asymmetric dipole about its midpoint, results in a net motion of the center of charge. Hence, these are not physically realistic systems. However, the interplay of the both these effects are observed in the real system in which an asymmetric dipole must rotate asymmetrically in order to preserve the position of the center-of-charge in the external field, and thus, though unrealistic, serve to further understanding of the effect of orientation on configurational energy.

The first effect is due to asymmetrically rotating the dipole by an angle φ. One can observe the result of this effect by considering a dipole where the two poles are of equal charge and forcing the system to rotate asymmetrically. The resulting potential is shown in the left panel of Figure 8. The transverse decays are still the most favorable, (though the minimum energy configurations have been shifted toward 180° decay), but here the 180° decay is much lower energy than the 0° decay. The effect of the 180° decay is to position the particle that is farther from the center-of-rotation farther from the PLF*.

The result of the asymmetry of the dipole (the second effect) can be examined by considering an asymmetric dipole (e.g. ^{7}Be, ^{4}He) and rotating it about the midpoint of the dipole rather than the center-of-charge. The right panel of Figure 8 shows the resulting potential as a function of the orientation of this dipole. Again, the lowest energy configuration is the transverse decay, (though shifted toward 0°) and the 180° decay is much less favorable than the 0° decay. Decay at 0° positions the ^{7}Be farthest from the PLF*.

Together, the effects seen in the two panels of Figure 8 explain the trend in Figure 7. For the real system, in "near" configuration, the more highly charged particle is closer to the PLF*, which is shown to be unfavorable in the right panel of Figure 8. In the "far" configuration, the particle further from the center of rotation is closer to the PLF*, which is shown to be unfavorable in the left panel of Figure 8. Thus the real system shows a high potential in the both the "near" and "far" configurations, with minimum energy for transverse decay.

The result of this potential is to preferentially orient the dipole in the field of the PLF* as the dipole is forming, thus making transverse decay more likely. This effect is

most important close to the PLF*. As seen in Figure 7, different orientation can correspond to a difference of as much as 3 MeV at a distance of 12 fm. As the angle is decay may have a large impact on the kinetic energy of the particle of interest, the anisotropy of the decay is an important consideration.

Modeling Proximity Decay

To investigate whether the physical scenario previously proposed can semi-quantitatively explain the observed data, we have developed the proximity decay model. The nomenclature used is illustrated in Figure 4. A computer simulation is used to numerically integrate the differential equations describing the motion of the three body problem which cannot be solved analytically. This simulation takes an initial configuration of two charged particles, the PLF* and the emitted particle, and numerically integrates the differential equation describing their relative motion using an implementation of the fourth order Runge-Kutta method. After an initially specified lifetime has elapsed, the two-body integration terminates. The emitted particle is replaced by two daughter particles at a specified relative distance from each other. The equation of motion describing this three-body system is then numerically integrated until the accelerations (and thus the inter-particle forces) are negligible for each particle. The final positions and velocities of the three particles are then returned by the integration routine and the transverse energy of the particle of interest is calculated.

The initial velocities of the emitted particle and the PLF* are determined by conservation of momentum and the following equation describing the average total kinetic energy of the pair in their center of mass frame.

$$\langle KE_0 \rangle = 2T_{PLF*}$$

$$T_{PLF*} = \sqrt{\frac{E^*_{PLF*}}{a}}$$

$$a \equiv level\_density = \frac{A_{PLF*}}{9}$$

At the moment of decay, the initial positions of the daughter nuclei are determined by preserving center-of-charge distance and positioning the particles as touching spheres. The center-to-center separation of the daughter nuclei is given by:

$$r_0 = 1.2\left(A_1^{1/3} + A_2^{1/3}\right) + 2 \quad \text{(fm)}$$

where A_1 and A_2 are the mass numbers of the decay products.

The relative velocities of the two daughters are determined by conservation of momentum and energy. The total initial kinetic energy of the pair in their center of mass frame is given by

$$KE_0 = E^*_{EP} + Q_{decay} - V_{touching\_spheres}$$

This equation can be modified by subtracting a term ΔV_{dipole} to account for tidal effects as previously discussed. The excitation energy of the emitted particle is taken to be a constant based on the excitation of the PLF* excitation, which, for simplicity, is also taken to be a constant.

The decay of the emitted particle is taken to be isotropic. The emission is taken to be only in one direction since the most relevant quantity is the direction of decay with respect to the emission direction.

The identity of the PLF* before emission is taken to be Z=41 (Nb) [1] and is given a mass number A=97 to maintain the same N/Z ratio as the projectile [1]. The emitted particle is chosen such that its proton decay or alpha decay yields one of the N<Z

nuclides Figure 1. A reasonable lifetime of the emitted particle is obtained from Γ, the energy width of an excited state, by using the uncertainty relation between time and energy:

$$\Gamma\tau = \hbar$$

where τ is the mean lifetime. For an excited state with an energy width of 2 MeV, the mean lifetime of the particle is $6.58*10^{-22}$ seconds. A particle moving at 1/3 c would cover 32.9 fm in that time, thus the tidal effect will have a significant impact.

A more detailed simulation may be developed by statistically sampling distributions for several of the initial conditions, namely:

a) The initial velocity of the emitted particle can be obtained by sampling the Maxwell-Boltzmann distribution described by the temperature of the PLF*. Though strictly speaking, the excitation energy of the PLF* should be obtained by statistical sampling, the trend in enhancement of neutron deficient isotopes is expected to be more clearly seen if the excitation is a fixed value.

b) The excitation of the emitted particle (E^*_{EP} above) should be taken from a statistical sampling of the Maxwell-Boltzmann distribution given by T_{PLF*} as well.

c) The direction of decay can be obtained by sampling an anisotropic distribution determined by the tidal effect.

Careful testing of the simulation code is of utmost importance. First, the simulation must conserve momentum. Figure 9 shows the momentum of a two-body/decay/three-body system. The total momentum of the particles always equals the initial momentum of zero. The discontinuity at the time of decay is a result of replacing

the emitted particle with its two daughters, which are given the same velocity as their parent, thus each have a different (and lesser) momentum.

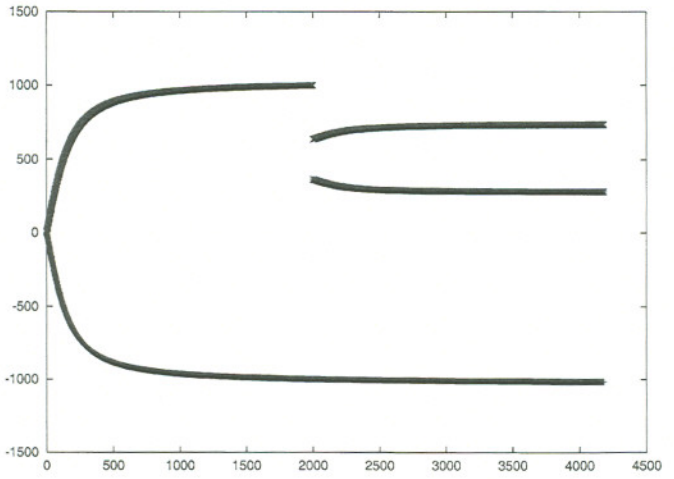

Figure 9
Momentum (MeV/c) as a function of time (fm/c) for a three body simulation.

Mass and energy must also be conserved. For a system involving no decay, only kinetic and potential energy are involved:

$$KE_0 + V_0 = KE_f + V_f$$

For a system involving decay, the following equation must be satisfied, which accounts for the potential of the two daughters of the emitted particle and their additional kinetic energy at the instant of decay:

$$KE_0 + V_0 + E^*_{EP} + Q_{decay} = KE_f + V_f$$

For the two body system, the simulation is accurate to a few parts in 10^6. For the 2body/decay/3body system, if the lifetime is long (>100 fm/c), the error is also on the order of a few ppm. For shorter lifetimes, the error rises to a few MeV due to the

potential difference of the dipole's interaction with the PLF* to the monopole's interaction with the PLF*. It is expected that this problem can be overcome by including the ΔV_{dipole} term where appropriate (specifically in assigning velocities to the daughter nuclei at the instant of decay).

In preparation for future work in which initial conditions will be obtained from statistical sampling, I have developed subroutines to allow efficient sampling. In sampling, it is necessary that the collection of values obtained from sampling accurately reproduces the distribution being sampled. Figure 10 shows that the normalized histogram obtained from sampling a Boltzmann distribution matches the normalized input Boltzmann distribution.

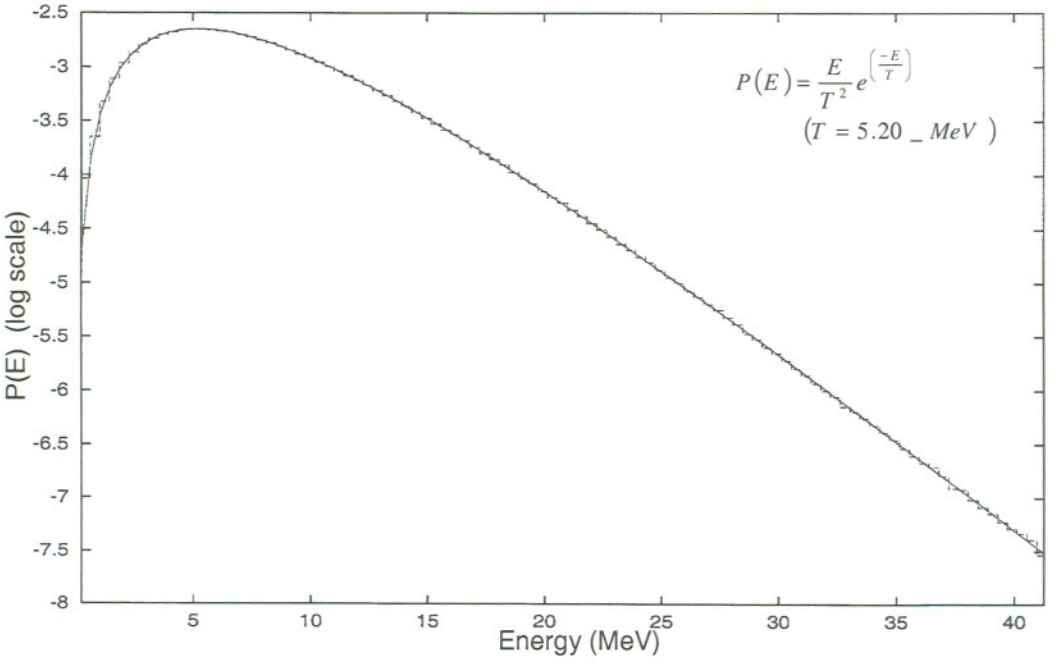

Figure 10

The normalized distribution of points obtained from sampling a Maxwell-Boltzmann distribution reproduces the input distribution. The solid curve is the input Maxwell-Boltzmann distribution, and the dashed line shows the bin-wise distribution of points. The input distribution was sampled 1e6 times and 100 bins in energy were used.

Many of the results that the simulation has produced have been surprising, such as the strong dependence of $\langle E_T \rangle$ on decay angle, but upon close examination, the results appear to physically sensible and correct. In such a case, the results must be analyzed carefully, though the simulation has passed all tests thus far. Full simulation using sampling of all necessary parameters with enough events to allow a statistically significant analysis is anticipated.

SECTION II: Preparation for an upcoming Experiment (GANIL E432)

Prior to any experiment, it is necessary to test and understand the performance of all detectors that will be used in the experiment. Categorizing the problems with the detectors is the first step to either fixing or replacing non-functioning detectors.

An upcoming experiment will utilize two detector arrays: FIRST (Forward Indiana Ring Silicon Telescope) and LASSA (Large Area Silicon Strip Array). Both make use of the dE-E technique for particle identification. The dE-E technique is based upon the relationship between the total energy of a charged particle and the rate of its energy loss dE/dx it incurs in traversing a slice of matter dx thick. In utilizing this technique, one arranges two detectors in a stack. The incident particle passes through the first detector in which it deposits some of its energy (dE). It then enters the second detector, where it stops, depositing the remaining energy (E). The rate of energy loss of a charged particle or fragment in a medium obeys (to a good first order approximation):

$$\frac{dE}{dx} \propto \frac{Z^2 A}{E}$$

where Z and A are the charge and mass of the particle respectively, E is its kinetic energy and dx represents the thickness or distance traversed by the particle. (Bethe's formula, based on quantum mechanical calculations, describes the rate of energy loss more accurately. For non-relativistic velocities, the above equation is a very good approximation.) Since the hyperbolic relationship between dE and E is dependent on the mass and charge, every unique pair of mass and charge numbers describe a unique hyperbola, allowing particle identification.

Ion passivated silicon detectors Si(IP) are used to measure dE signals, and the E signal can be obtained from either a scintillator crystal of cesium iodide doped with thallium [CsI(Tl)] for light charged particles or a second silicon detector for heavier fragments. Scintillation from the crystals is converted to an electronic signal by photodiodes optically coupled to the back of each crystal. The FIRST array [3] covers forward angles from 2.1° to 27.1° in the lab. It is comprised of three telescopes: T1, T2 and T3 in order of increasing azimuthal angle. Telescope T1 is comprised of two highly segmented annular Si(IP) detectors for accurate position information backed by 16 CsI(Tl) crystals. T2 and T3 each have one highly segmented Si(IP) detector backed by CsI(Tl) crystals. The Si(IP) detectors of T1 are segmented into 16 pies (which match the CsI(Tl) crystals) on the junction side and 48 concentric rings on the ohmic side. The Si(IP) detectors of T2 and T3 are segmented into 16 rings (segmented into quadrants) and 16 pies. At the most forward angles, a higher angular resolution is necessary to resolve particles due to the kinematic focusing of heave ion beams typically used. The high segmentation of T1 affords this resolution. T1 used dual (stacked) Si(IP) detectors so that heavier fragments can be identified. As heavy fragments lose energy more rapidly than light particles, the first detector is thin enough to allow most heavy fragments to pass through so that the E signal can be obtained from the second Si(IP).

The LASSA array [4] is comprised of eight square trapezoid telescopes arranged in a ring at mid-angles ($32.2° \leq \theta \leq 46.8°$). Each LASSA telescope consists of two stacked Si(IP) detectors. The thinner front detector is segmented into 16 strips, while the thicker backing detector is segmented into 16 horizontal strips and 16 vertical strips.

Backing the Si(IP) detectors are four CsI(Tl) crystals that function as stopping detectors for energetic particles.

In preparation for E432, I have tested both detectors and their associated electronics – in particular their pre-amplifiers (PA). Specifically, I have tested the silicon detectors for FIRST, the CsI(Tl) for FIRST, and the CsI(Tl) for LASSA.

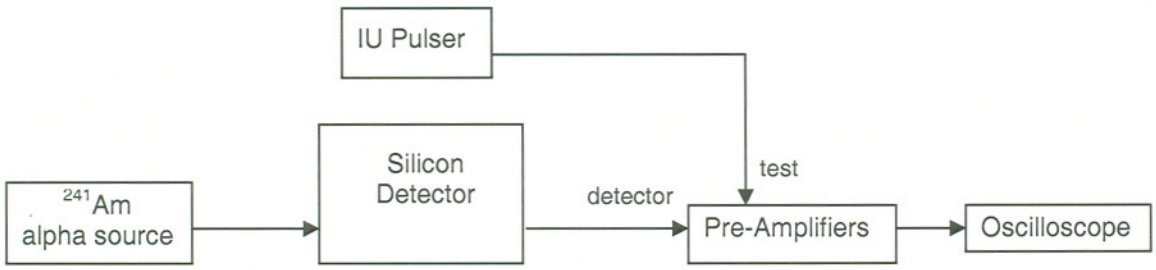

Figure 11 *schematic of electronics chain used to test FIRST silicon detectors.*

FIRST Silicon

A brief schematic for the electronics chain used in testing is shown in Figure 11. The FIRST silicon detectors were tested using an alpha source (^{241}Am). The T2 detector was connected to the input of a charge integrating PA. The stability of the PA was simultaneously monitored by sending a voltage pulse into the test input of the PA [5]. The resulting output signal for each channel due to both the input pulser and the detector was examined via an oscilloscope. By comparing the response to the pulser and the detector signals, one could diagnose if a problem was due to the detector or to a faulty PA.

With the alpha source illuminating the detector in the chamber at high vacuum ($\approx 10^{-5}$ torr), a voltage was applied to the detector. This reverse biasing of the detector

causes the depletion zone of the junction to encompass the entire detector volume to ensure complete charge collection of any ionization in the detector and also results in reduced thermal noise in the detector. The T3 detector was tested in the same manner as T2. In testing T1-dE, the PA for T2 were used, as the PA dedicated to T1 during the experiment have low gain (matched to the energy deposit expected for projectile-like fragments). The T1-E detector remains to be tested.

The results for these tests of the FIRST silicon detectors and PA are summarized in the appendix. All PA are functioning for T2. All detector channels on T2 are working as well, though there appears to be a noise problem for some channels. Since channel 16 is noisy for all four ring quadrants, this noise may arise from a common problem in the PA housing.

In T3, one channel didn't show either a signal from the detector or from the pulser. It is likely that the PA for this channel is dead. We anticipate replacing this PA and testing this channel again. Another two channels show pulser and alpha peaks at half the amplitude of the other channels. The two preamps for these channels must have a different gain, and can also be replaced. Another channel shows a pulser peak but not an alpha peak. To diagnose this problem correctly, the bias was turned off, the chamber brought to atmosphere, and light was allowed to hit the detector. The photons cause a signal in other channels, but not in the channel under investigation. It is likely that the wire-bond for this strip which transmits the signal from the silicon to the output connector is broken. Physical investigation of the wire-bond under a 30x optical microscope can reveal if this is the case. If the wire-bond is broken, it will have to be

replaced by bonding a new wire. The noise level on a few other channels is very large and will have to be investigated further and remedied.

All ring channels for T1dE show an alpha signal except one, which is too noisy to see any alpha signal of the expected magnitude. Other noisy channels must be investigated as well, but the primary concern is the T1dE pies. All of these channels exhibit inordinate amounts of noise. The source of this noise has been traced back to the "clean" power supply at the wall, and while changing the grounding of the PA cans to the chamber alters the noise, a stable and satisfactory noise level has yet to be achieved.

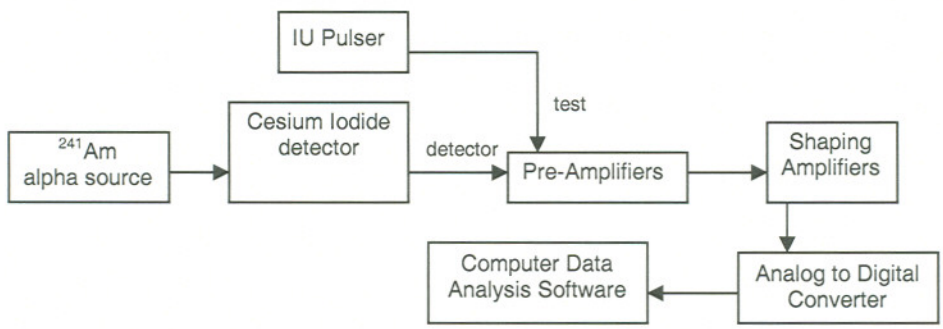

Figure 12
Electronics chain used in test of FIRST CsI

FIRST Cesium Iodide

A brief schematic for the electronics chain used in testing is shown in Figure 12. The cesium iodide detectors of FIRST (with their photodiodes) and their PA were tested using an alpha source (^{241}Am) and a pulser. The photodiodes leads had already been soldered to co-axial connectors (SMC) and thus this test is also a test of the solder connection. The connectors were cabled to the appropriate PA board. The PA for the CsI(Tl) are situated inside the vacuum chamber to minimize the influence of cable

capacitance. The signal from PA was shaped into a gaussian-like signal using a shaping amplifier to allow digital conversion with an analog-to-digital converter (ADC). The signal from the ADC was read out by the computer while the signal from the shaping amplifier was examined via an oscilloscope.

The results for FIRST CsI(Tl) are shown in the appendix. T2 is fully functional. T1 shows pulser for all channels, and three channels show no alpha signal. This may be due to a bad connection with the photodiode leads or to poor optical coupling between the scintillator, light guide, and photodiode; though the latter is less likely. T3 also shows pulser signal for all channels, and shows no alpha signal for one channel. Two other channels are very noisy, and another exhibits sparking.

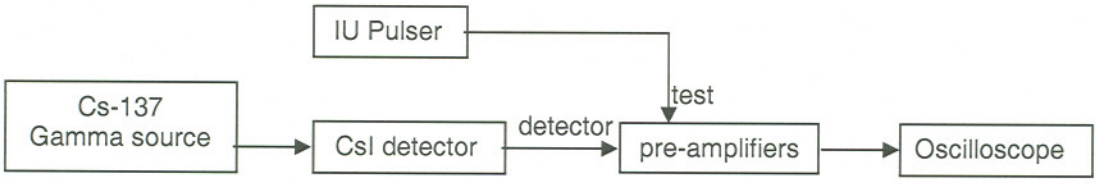

Figure 13
Electronics chain used in test of LASSA CsI

LASSA Cesium Iodide

A brief schematic for the electronics chain used in testing is shown in Figure 13. The cesium iodide detectors of LASSA were tested. These tests were carried out on the bench-top (at ambient pressure) to save the time it would have required to set up all telescopes in the vacuum chamber. A gamma source (^{137}Cs) was used in place of the alpha source due to the longer range of gamma rays in air. A pulser was connected to the test input of the PA. The output of the PA was monitored directly on the oscilloscope.

Before biasing the photodiodes, the detectors were covered with a black felt cloth to reduce ambient light. To further lessen the exposure of the photodiodes to ambient light, the room lights were extinguished and the window shades were closed. Light can severely damage a biased detector or a biased photodiode. Some detectors were biased in groups, while others were tested individually; this should not affect the functionality of any detector, though the current drawn by the bias will be proportional to the number of photodiodes biased.

One whole telescope (L3) cannot be safely biased, suggesting there is a short to ground for the bias. Telescope L4 crystal 1 appears to have a dead PA, as there is neither a detector nor pulser signal. L6 crystal 1 shows only pulser signal, possibly due to a poor solder between the photodiode and the connector.

In conclusion with regard to detector testing, there is much yet to be done. Several channels can be recovered easily by changing out a pre-amplifier. Several more channels can be recovered by checking and re-soldering photodiode leads and by examining the optical coupling for flaws. The most significant problem is the general noise. A better method of grounding the pre-amplifier boards and the detectors needs to be found and understood.

APPENDIX
status of detectors

FIRST Silicon, T1

Bias:	(-)65 V on rings
Leakage:	5.95 μA
Signal:	15 mV
Noise:	5 mV

T1 dE – Pies

Channel	Pulser	Signal	Comments
1-16	?	?	too noisy to see

T1 - R 1-16

Channel	Pulser	Signal	Comments
1-16	y	y	OK

T1 - R 17-32

Channel	Pulser	Signal	Comments
1-12,15,16	y	y	OK
13,14	y	y	noisy

T1- R 33-48

Channel	Pulser	Signal	Comments
1,5-16	y	y	OK
2	?	?	extremely noisy
3	y	y	noisy
4	y	y	somewhat noisy

FIRST Silicon, T2

Bias:	(-)35 V on rings
Leakage:	1.18 μA
Signal:	16 mV
Noise:	1.7mV

T2 – Pies			
Channel	**Pulser**	**Signal**	**Comments**
1	y	y	very noisy
2-16	y	y	OK

T2 – QA			
Channel	**Pulser**	**Signal**	**Comments**
1-12,14,15	y	y	OK
13	y	y	very noisy
16	y	y	somewhat noisy

T2 – QB			
Channel	**Pulser**	**Signal**	**Comments**
1-15	y	y	OK
16	y	y	somewhat noisy

T2 – QC			
Channel	**Pulser**	**Signal**	**Comments**
1-15	y	y	OK
16	y	y	somewhat noisy

T2 – QD			
Channel	**Pulser**	**Signal**	**Comments**
1-15	y	y	OK
16	y	y	somewhat noisy

FIRST Silicon, T3

Bias:	(-)65 V on rings
Leakage:	2.17 μA
Signal:	14 mV
Noise:	5 mV

T3 – Pies

Channel	Pulser	Signal	Comments
1-4,6-8,10-15	y	y	OK
5	y	y	very noisy
9	y	y	noisy

T3 – QA

Channel	Pulser	Signal	Comments
1-13,15,16	y	y	OK
14	y	NO	no signal. No photons.

T3 – QB

Channel	Pulser	Signal	Comments
1-5,7-11,13-16	y	y	OK
6,12	y	y	very noisy

T3 – QC

Channel	Pulser	Signal	Comments
1,4-15	y	y	OK
2	y	y	signal low by factor of 2
3	y	y	signal low by factor of 2
16	y	y	noisy

T3 – QD

Channel	Pulser	Signal	Comments
1-13,15,16	y	y	OK
14	NO	NO	pre-amp dead

FIRST CsI

T1 CsI

Bias:	25 V
Current:	74 nA
Alpha signal:	130 mV
noise:	9 mV

photodiode	pulser	signal	comment
1-10,12,13,15	y	y	OK
11	y	NO	no alpha signal
14	y	NO	no alpha signal
16	y	NO	bad connection, no noise, no alpha

T2 CsI

Bias:	25 V
Current:	83 nA
Alpha signal:	150-200 mV
noise:	30 mV

photodiode	pulser	signal	comment
1-16	y	y	OK

T3 CsI

Bias:	25 V
Current:	83 nA
Alpha signal:	110-190 mV
noise:	10 mV

photodiode	pulser	signal	comment
1-3,5,8-13,15,16	y	y	OK
4	y	NO	no alpha signal
6	y	y	sparking
7	y	y	noisy: 30 mV
14	y	y	noisy: 30 mV

LASSA CsI

4 telescopes at once

Bias:	25 V
Current:	60 nA
±12V Current:	0.12 A, 0.15 A
Signal:	20 mV
Noise:	10 mV

Telescope	Crystal	Pulser	Signal	comment
L2	1-4	y	y	OK
L5	1-4	y	y	OK
L6	1	y	X	no gamma, 5 mV noise
	2-4	y	y	OK
L8	1-4	y	y	OK

2 telescopes at once

Bias:	25 V
Current:	30 nA
±12V Current:	0.07 A, 0.08 A
Signal:	20 mV
Noise:	10 mV

Telescope	Crystal	Pulser	Signal	comment
L4	1	NO	NO	no sig, no pulser, no noise
	2-4	y	y	OK
L1	1-4	y	y	OK

1 telescope at once

Bias:	25 V
Signal:	20 mV
Noise:	10 mV

Telescope	Crystal	Pulser	Signal	comment
L7	1-4	y	y	OK

LASSA 3 may have a short related to bias

Bias (V)	Current (nA)
0.5	52
1.0	76
1.5	106
2.0	147
-0.5	LARGE

References:

1. S. Hudan *et al*, submitted Phys Rev C (2005)
2. Yanez *et al*, Phys Rev C **68** 011602 (2003)
3. T Paduszynski *et al*, in press, Nucl Instr Meth A (2005)
4. B Davin *et al*, Nucl Instr Meth Phys Res Section A **473** 301 (2001)
5. A Wagner *et al*, Nucl Inst and Meth A **456** 290 (2001)